Author/s:
McCormick, CA;Corlett, H;Roberts, NMW;Johnston, PA;Collom, CJ;Stacey, J;Koeshidayatullah, A;Hollis, C

Title:
U-Pb geochronology reveals that hydrothermal dolomitization was coeval to the deposition of the Burgess Shale lagerstätte

Date:
2024-12-01

Citation:
McCormick, C. A., Corlett, H., Roberts, N. M. W., Johnston, P. A., Collom, C. J., Stacey, J., Koeshidayatullah, A. & Hollis, C. (2024). U-Pb geochronology reveals that hydrothermal dolomitization was coeval to the deposition of the Burgess Shale lagerstätte. Communications Earth and Environment, 5 (1), https://doi.org/10.1038/s43247-024-01429-0.

communications earth & environment

Article

https://doi.org/10.1038/s43247-024-01429-0

U-Pb geochronology reveals that hydrothermal dolomitization was coeval to the deposition of the Burgess Shale lagerstätte

Cole A. McCormick[1], Hilary Corlett[2], Nick M. W. Roberts[3], Paul A. Johnston[4], Christopher J. Collom[4], Jack Stacey[1], Ardiansyah Koeshidayatullah[1,5] & Cathy Hollis[1]

Fault-controlled, hydrothermal dolomitization often occurs at margins between shallow-water carbonate platforms and deep-water sedimentary basins. In western Canada, for example, the platform margin between the Cathedral Formation and the Burgess Shale Formation has been dolomitized at temperatures up to ~200 °C, with local magnesite, talc, and clinochlore mineralization. At the same time, the Burgess Shale Formation includes exceptional fossils that provide key evidence of the radiation of the animal phyla during the Cambrian Period (541 to 485.4 Ma). This lagerstätte and Mg-rich minerals within the adjacent and underlying strata, however, have been critically understudied. Here we show, using carbonate U-Pb geochronology, that western Canada was tectonically active and subject to hydrothermal dolomitization during the Middle Cambrian (Miaolingian Epoch) to Middle Ordovician (488.1 ± 18.8 Ma). These results extend the latest stages of rifting along the western margin of Laurentia into the Paleozoic, while also suggesting that the dolomitization of the Cathedral Formation occurred at the same time as the deposition of the Burgess Shale lagerstätte.

The rapid evolution and diversification of marine life during the Cambrian Period (541 to 485.4 Ma) is a defining moment in the geological record due to the radiation of the animal phyla, alongside the increased complexity of their body plans, locomotory systems, and behaviours (Fig. 1A)[1–4]. In the Western Canada Sedimentary Basin (WCSB), for example, the Burgess Shale Formation (Middle Cambrian; Miaolingian Epoch; 509 to 497 Ma) includes several fossil lagerstätten that were inscribed on the UNESCO World Heritage List to conserve world-class examples of early annelids, arthropods, chordates, ctenophorans, and molluscs (Fig. 1B–F), often including the preservation of soft-bodied organisms and their internal tissues[5–8]. Over a century of research has been conducted since Charles Walcott's discovery of these sedimentary rocks and fossils in 1909[5], with similar Burgess Shale-type deposits now documented worldwide[9,10]. As a result, a vast literature has amassed on the Burgess Shale lagerstätte, but these studies have almost exclusively focused on the taxonomy, paleoecology, and taphonomy of these fossils[5–8]. In particular, the relationships between these fossils and the shallow-water carbonate platforms that bound the Burgess Shale Formation have been critically understudied.

Margins between shallow-water carbonate platforms and deep-water sedimentary basins are often structurally controlled[11,12] and can influence the syn- to post-depositional flow of diagenetic fluids[13,14]. Middle Cambrian strata in western Canada record a lateral platform-to-basin transition between the Cathedral Formation and the near age-equivalent Burgess Shale Formation (Fig. 1B, C), where the margin of the carbonate platform was controlled by the syn-depositional reactivation of deep-rooted basement faults[15–20]. On the platform, the shallow-water strata that comprise the Cathedral Formation have been widely used as exemplars for hydrothermal dolomitization[21] because this replacement reaction occurred at temperatures up to ~200 °C, which were significantly greater than the ambient

---

[1]Department of Earth and Environmental Sciences, The University of Manchester, Manchester M13 9PL, UK. [2]Department of Earth Sciences, Memorial University of Newfoundland; St. John's, Newfoundland A1C 5S7, Canada. [3]Geochronology and Tracers Facility, British Geological Survey; Environmental Science Centre, Nottingham NG12 5GG, UK. [4]Department of Earth and Environmental Sciences, Mount Royal University, Calgary, Alberta T3E 6K6, Canada. [5]Department of Geosciences, King Fahd University of Petroleum and Minerals, Dhahran 31261, Saudi Arabia. e-mail: cole.mccormick@psu.edu

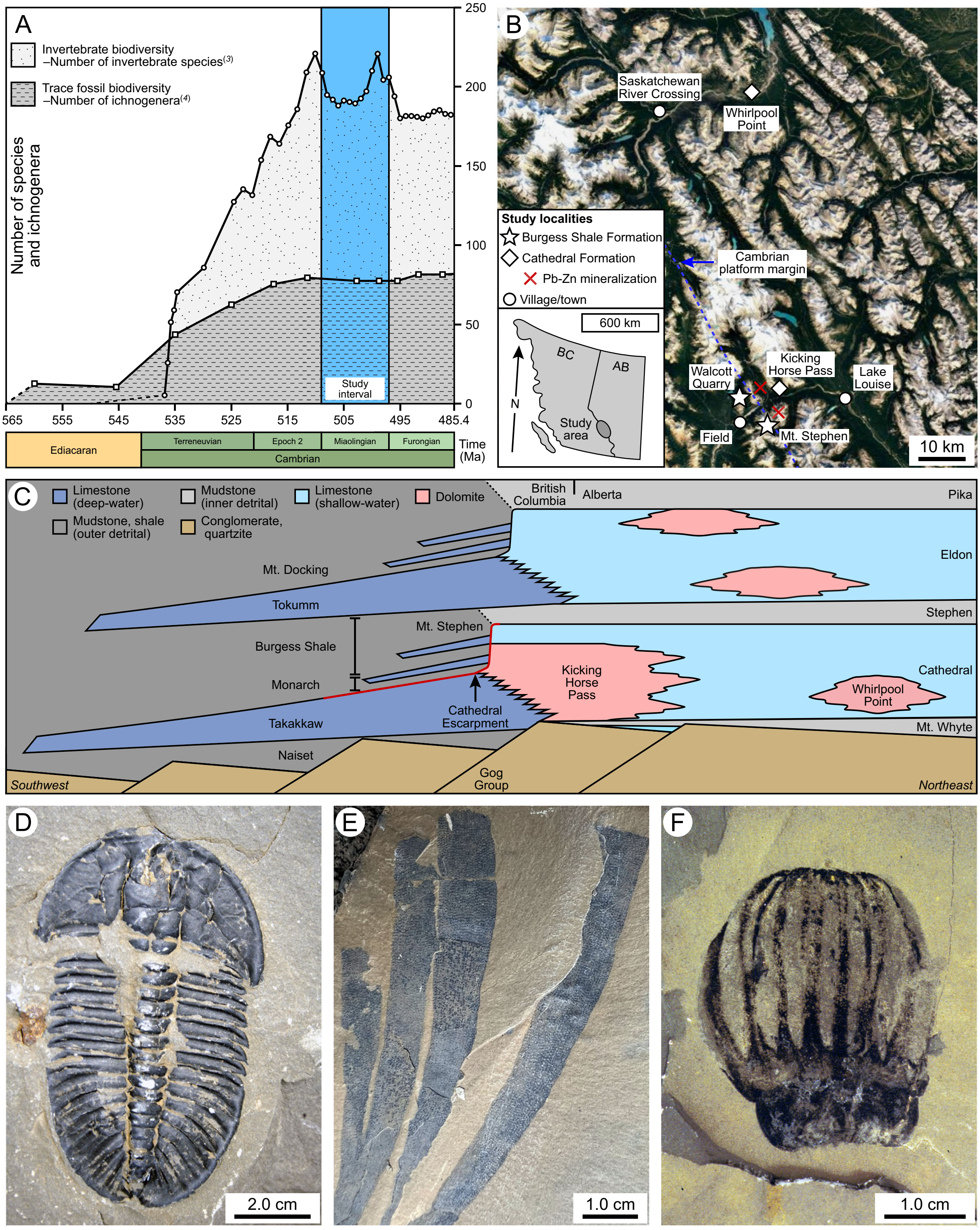

Fig. 1 | For over 100 years, Cambrian fossils in western Canada have provided a foundation for our understanding of early marine life on Earth. **A** Ediacaran to Cambrian global diversity curves showing the standing number of invertebrate species[3] and trace fossils[4]. **B** Location of the study area, and (**C**) schematic cross-section of the Middle Cambrian (Miaolingian Epoch) strata in the southern Rocky Mountains, western Canada[16,33]. Localities that were investigated include Mt. Stephen (51°23'34.7“N, 116°25'39.5“W), the Kicking Horse Pass (51°26′11.5″N, 116°22′48.5″W), and Whirlpool Point (52°00′07.5″N, 116°28′13.5″W). **D**–**F** Examples of fossilized biota in the Burgess Shale Formation, including (**D**) *Ogygopsis klotzi*, a trilobite; (**E**) *Vauxia* sp., a sponge, and (**F**) *Ctenorhabdotus capulus*, a comb-jelly.

temperature of the host-rock at the time of dolomitization[22–26]. These dolomite geobodies are located proximal to magnesite, talc, and Mississippi-Valley-type (MVT) deposits along the platform margin (Fig. 1B, C), with dolomite, talc, and clinochlore reported within, or adjacent to the Burgess Shale Formation[18–20]. Indirect paleomagnetic and geochemical evidence led several studies to propose that dolomitization occurred during the Antler (Devonian to Mississippian) or Laramide (Cretaceous to Paleocene) orogenies[27–29]. In that case, mineralization post-dated the deposition of the lagerstätte by 100's of millions of years, at a depth of several kilometers, and cannot be linked. Conversely, these Mg-rich fluids have also been interpreted to be syndepositional, with brine seeps that breached the seafloor and gave rise to mud volcanism, increased microbial activity, and the concentration of animals along their periphery[19–21].

Using carbonate U-Pb geochronology, this interdisciplinary study constrains the timing of fault-controlled, hydrothermal dolomitization along the platform margin between the Cathedral Formation and the Burgess Shale Formation. Given that dolomitization is spatially associated with faults that intersect Cambrian strata in the southern Rocky Mountains of western Canada[22–30], these radioisotopic ages can significantly bolster our understanding of either (1) extensional tectonism along the western margin of Laurentia (Neoproterozoic), (2) the Antler Orogeny (Devonian to Mississippian), or (3) the Laramide Orogeny (Cretaceous to Paleocene). In the first case, where the transition from a rift basin to a passive margin is largely unconstrained, U-Pb geochronology also provides a direct test of the brine seep model of fossil communities within the Burgess Shale lagerstätte[18–21].

Results

Geological evidence of hydrothermal activity in western Canada

The western margin of Laurentia was tectonically active during the Middle Cambrian, when the Cathedral Formation and the near age-equivalent Burgess Shale Formation were deposited on a shallow-water carbonate platform and in a deep-water basin, respectively (Fig. 1C). Such tectonic activity is evidenced by the rapid thickening of the sedimentary strata towards the platform margin[15,16], alongside their decimeter-scale buckling and deformation[17]. The boundary between the platform to the northeast and the basin to the southwest was controlled by a syndepositional fault system that is associated with an erosional collapse feature, the Cathedral Escarpment (Fig. 1C)[31–33]. This escarpment resulted in a regional embayment to the northwest of Mt. Stephen (Fig. 2A), with > 150 m of topographic relief between the platform and the basin[31–33].

Deposited on the shallow-water carbonate platform, the Cathedral Formation comprises limestone and dolomite (Fig. 2B, C). The preserved biota on the platform is less diverse than in the basin, and the strata are dominated by microbial textures, coated grains, and bioturbated carbonate mudstone. Although the paleoecology of the platform has received limited attention, several studies have used petrographical and geochemical analyses to evaluate the mechanism of dolomitization[22–30]. Fluid inclusion and carbonate clumped isotope analyses indicate that the dolomite formed at temperatures up to ~200 °C[23,27], which led previous studies to suggest that dolomitization occurred 100's of millions of years after deposition, by fluid-rock reactions deep in the crust[28–30]. Conversely, recent studies have used textural evidence to demonstrate that dolomitization occurred in a shallow-burial setting[23–27]. Quartz grains in the Gog Group (Lower Cambrian; Terreneuvian to Epoch 2; 541 to 509 Ma), which underlies the Cathedral Formation, lack grain-to-grain contacts because the intergranular pores were filled with dolomite cement prior to burial[25]. Bedding-parallel stylolites crosscut individual dolomite crystals, which indicates that they formed before the lithostatic stress increased during burial[25]. These studies invoke normal-to-transtensional faults as conduits for hydrothermal fluids because these faults exhibit a first order control on the distribution of dolomite in the strata[23–27]. Critically, such petrographical evidence broadly constrains the timing of dolomitization to a shallow-burial setting, prior to the Antler Orogeny (Devonian to Mississippian), but it does not provide the resolution required to determine if the system was active at the same time as the deposition of the Burgess Shale lagerstätte.

Deposited in the adjacent deep-water basin, the Burgess Shale Formation comprises mudstone and shale, with minor limestone and dolomite (Fig. 2D–F). Another major tectonic feature, the Fossil Gully Fault Zone (FGFZ), was active during the Cambrian and was later reactivated, probably during the Laramide Orogeny, to thrust the Burgess Shale Formation against the Eldon Formation (Fig. 2D)[18–20]. On Mt. Stephen, the famous Trilobite Beds of the Burgess Shale Formation are situated next to the FGFZ (Fig. 2D–F), with a concentric zonation of five sedimentary facies, arranged from proximal to distal relative to the inferred fluid-source emanating from the fault zone: (i) clinochlore fills the fault, and where interbedded with shale and dolomite, contains rare trilobites; (ii) a black facies comprises thin-bedded shale with dense accumulations of *Ogygopsis klotzi* with low faunal diversity; (iii) a red facies features increased faunal diversity but reduced density; (iv) a more diverse green facies, with less density, includes trilobites with fewer claws of the dinocarid *Anomalocaris*; and (v) a brown facies with dispersed disarticulated trilobites, sponges, and molluscs that also includes barren intervals. Major element analyses have demonstrated that there is a decrease in Mg with increased distance from the FGFZ, with up to 27.2 wt% MgO in the clinochlore, intermediate values in the black and red facies, and 2.0 wt% MgO in the green facies[19,20].

Petrographical screening of samples for U-Pb geochronology

Based on transmitted light and cathodoluminescence microscopy (Fig. 3A, B), Middle Cambrian strata in western Canada include two phases of replacement dolomite (RD)[23–27]. RD1 comprises finely crystalline (20–150 μm), planar-euhedral dolomite that are oscillatory zoned with moderate-red luminescent cores and dull-red luminescent rims (Fig. 3C, D). RD2 comprises medium-crystalline (100–400 μm) planar-subhedral dolomite that are unzoned with mottled dull- to moderate-red luminescence (Fig. 3E, F). Based on cross-cutting relationships, RD2 post-dates RD1 and is spatially related to the occurrence of saddle dolomite (SD) in the strata[26]. Previous studies have demonstrated that RD2 formed by the recrystallization of RD1 (i.e., replacement of dolomite by new, thermodynamically stable crystals of the same mineralogy) due to (i) an increase in crystal size, (ii) an increase in stoichiometry and cation ordering, (iii) changes in trace element and stable isotopic composition, and (iv) an increase in fluid inclusion and clumped isotope temperatures[23–27]. Based on such petrographical screening, U-Pb geochronology was conducted on samples of RD1 from the Kicking Horse Pass ($n = 4$) and Whirlpool Point ($n = 8$) localities (Fig. 1C). There are also several phases of SD in the strata[23–27], but dating these later paragenetic stages is beyond the scope of this study.

U-Pb geochronology and timing of hydrothermal activity in western Canada

Twelve samples of RD1 were prepared as polished blocks and analysed by in situ laser ablation inductively coupled plasma mass spectrometry (Supplementary Data 1)[34–38]. RD1 crystals were specifically targeted if they (i) were larger than the diameter of the laser ablation spot (100 μm), (ii) did not have clinochlore or talc within their cleavage planes, and (iii) displayed no clear petrographical evidence of recrystallization[23–27]. Quoted U-Pb ages are lower concordia intercepts that were calculated from Tera-Wasserburg plots ($^{207}\text{Pb}/^{206}\text{Pb}$ vs. $^{238}\text{U}/^{206}\text{Pb}$), reported alongside their 95% confidence intervals (β) and mean square weighted deviation (MSWD)[34–36].

At the Kicking Horse Pass locality, directly at the margin between the Cathedral Formation and the Burgess Shale Formation, RD1 formed at 475.3 ± 21.8 Ma with an initial Pb isotopic composition of 0.8162 ± 0.0042 (Fig. 4A, C). However, recrystallization is prevalent at the Kicking Horse Pass[26] and these ages may reflect the subtle re-equilibration of the U-Pb system upon burial[35–37]. Samples from the Whirlpool Point locality, where recrystallization is less evident[23–27], indicate that RD1 formed at 488.1 ± 18.8 Ma with an initial Pb isotopic composition of 0.7467 ± 0.0033 (Fig. 4B, D). U-Pb geochronology reflects the timing of replacement, via

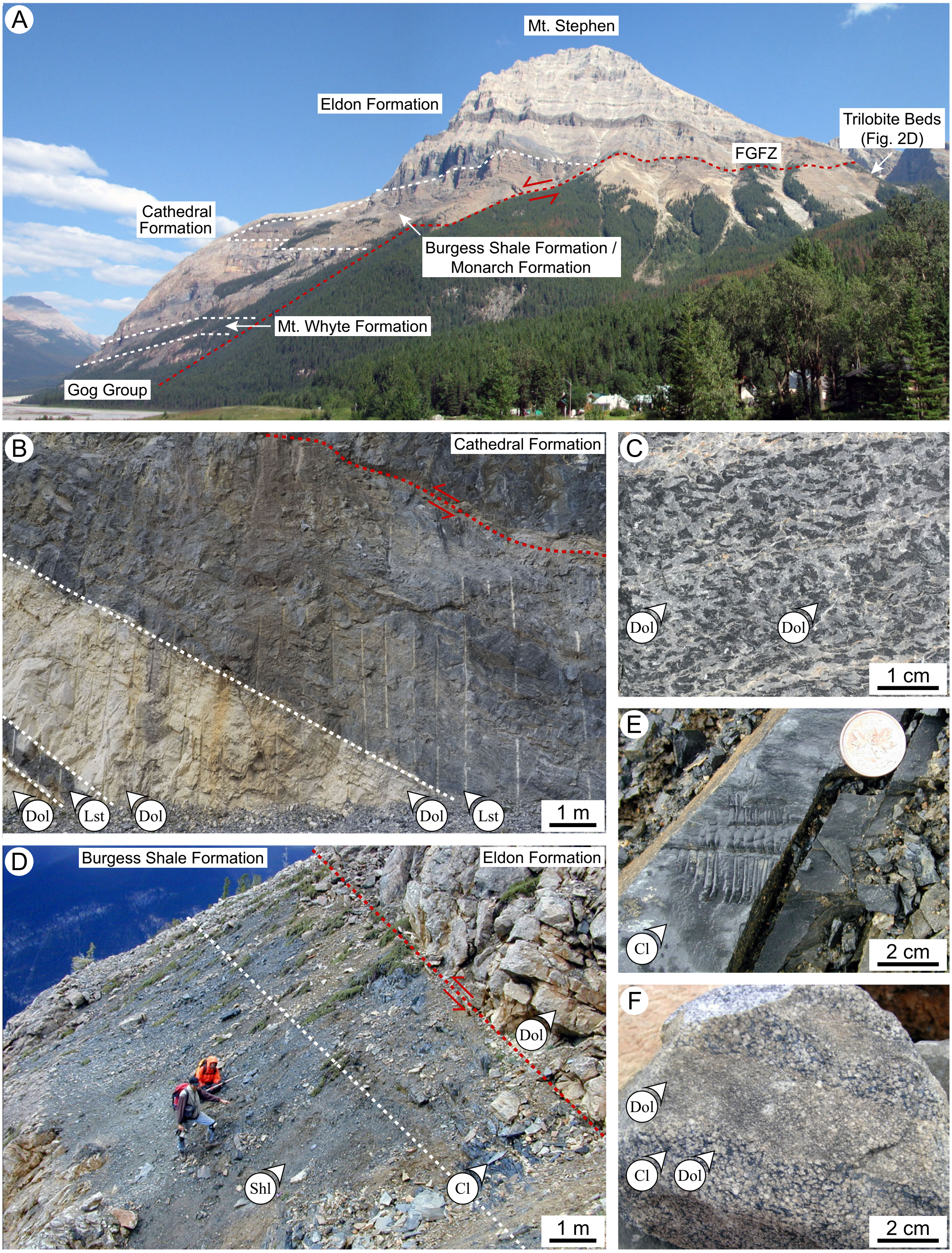

Fig. 2 | Geology of the Cambrian strata in the southern Rocky Mountains, western Canada. **A** Mt. Stephen as seen from Field, British Columbia. FGFZ = Fossil Gully Fault Zone. **B** Alternating units of limestone and dolomite in the Cathedral Formation at the Kicking Horse Pass locality. **C** Sample of dolomite from the Cathedral Formation that was used for U-Pb geochronology (photomicrographs shown in Fig. 3). **D** Contact between the Burgess Shale Formation and the Eldon Formation, with clinochlore in the FGFZ. **E** Natural mould of a trilobite fossil from the Burgess Shale Formation, showing the replacement of calcite by clinochlore. **F** Sample of dolomite and clinochlore from the Burgess Shale Formation. Lst limestone. Dol dolomite. Shl shale. Cl clinochlore.

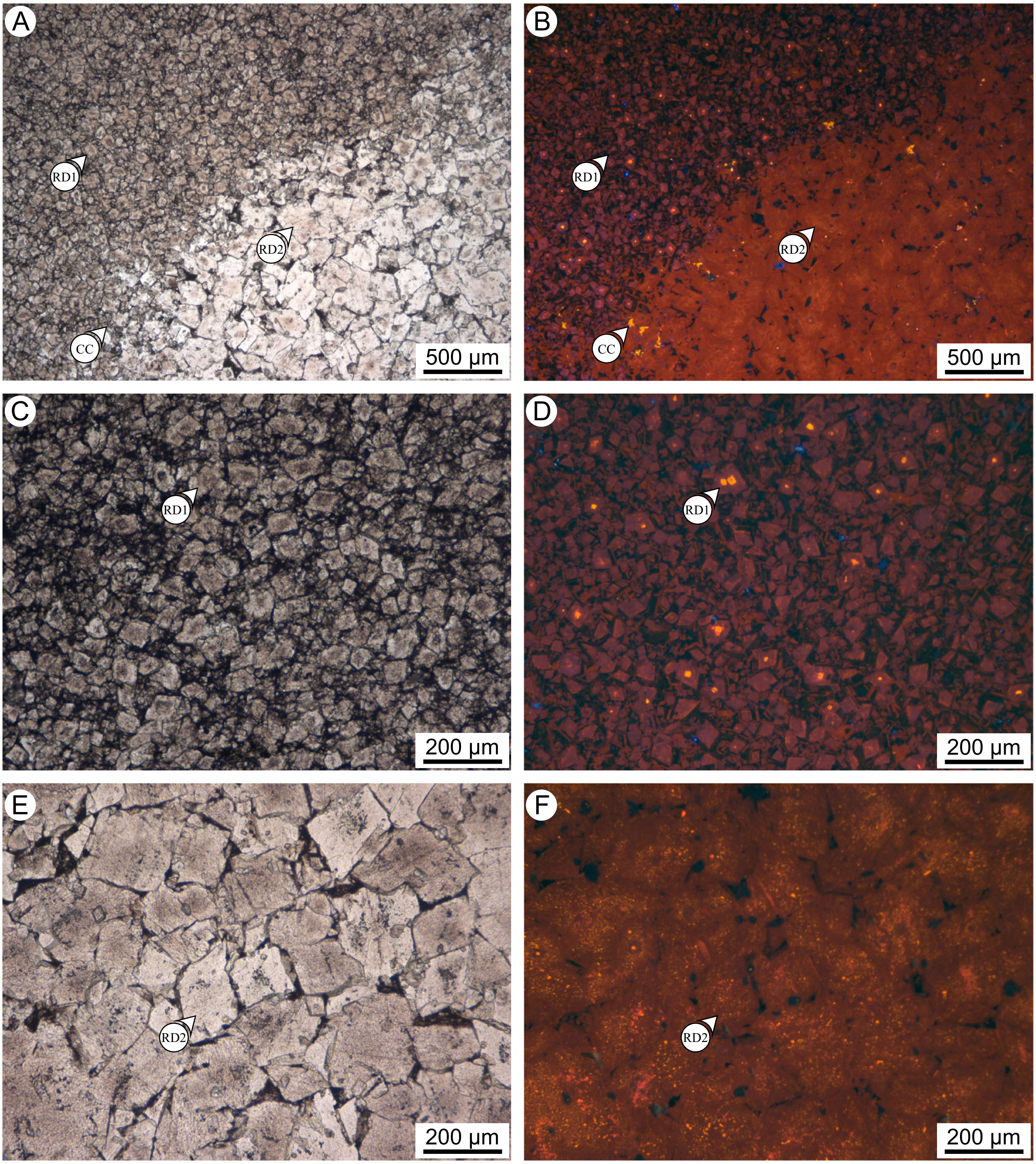

Fig. 3 | Pre-ablation petrographical characterization of a representative sample from the Kicking Horse Pass locality (Fig. 2B, C), showing transmitted light (left) and cathodoluminescence (right) photomicrographs. A, B Contact between RD1 and RD2, where (**C**, **D**) RD1 comprises oscillatory zoned, finely crystalline (20–150 μm), planar-euhedral dolomite, and (**E**, **F**) RD2 comprises unzoned, medium-crystalline (100–400 μm), planar-subhedral dolomite[23–27]. Relative to the Kicking Horse Pass, samples from Whirlpool Point comprise a greater proportion of RD1, but their petrographical characteristics are largely analogous. RD replacement dolomite. CC calcite cement.

dissolution-precipitation, which cannot occur before the original carbonate sediment was deposited. Thus, the upper and lower limits of the 95% confidence interval indicate that dolomitization was syn- to early post-depositional, with a gaussian distribution of age estimates from 506.9 to 469.3 Ma. These data demonstrate that the western margin of Laurentia was subject to fault-controlled, hydrothermal dolomitization during the Middle Cambrian to Middle Ordovician.

Discussion

Source(s) of Mg-rich brines for dolomitization

Fluid inclusion and clumped isotope analyses of RD1 demonstrate that dolomitization occurred at temperatures up to ~200 °C, which implies that these Mg-rich brines originated from a depth of at least 6–8 km[23–29]. Based on the burial history of Cambrian strata in the WCSB (Fig. 5A), there is no way to reconcile such deep burial conditions with our results from U-Pb

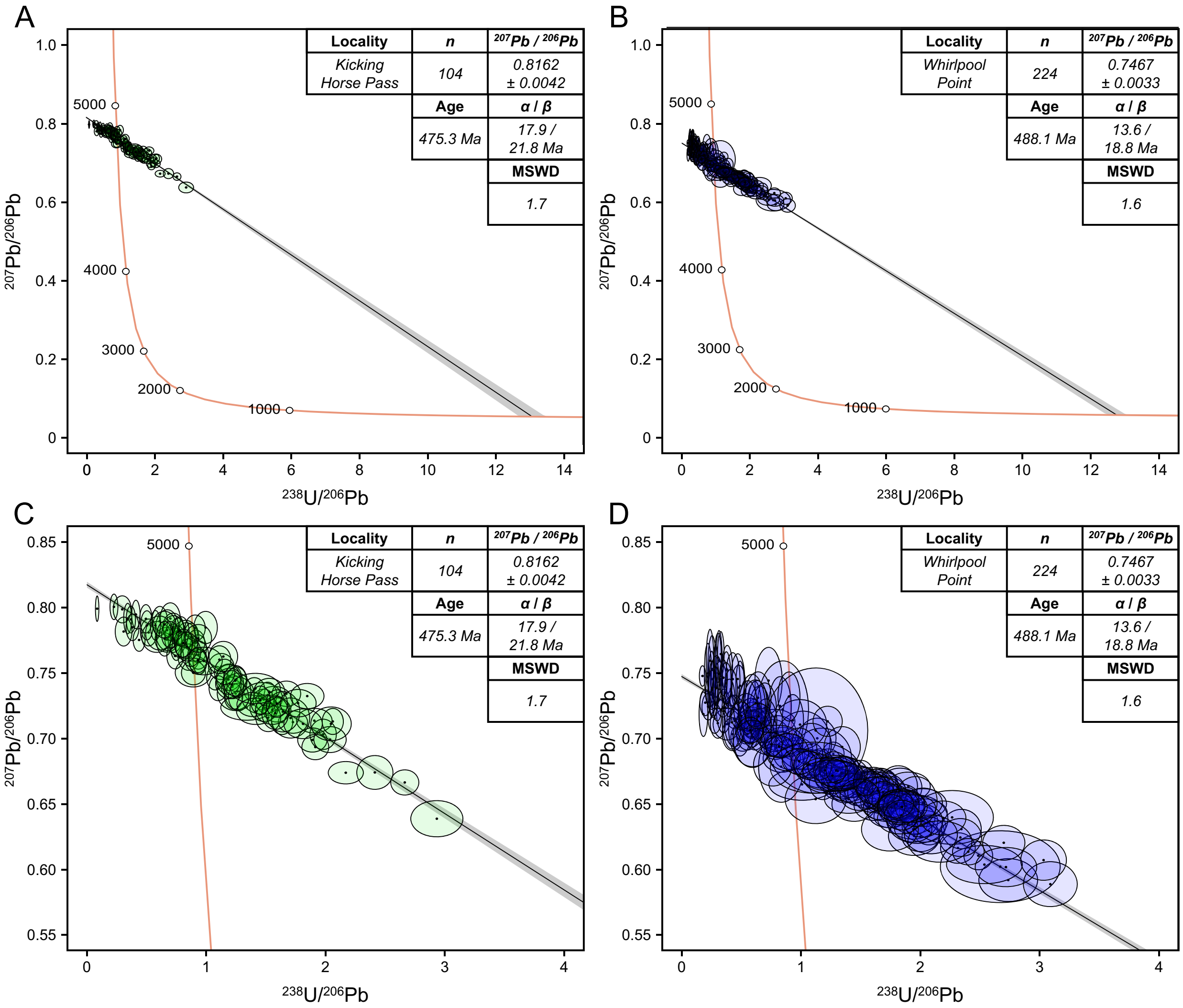

Fig. 4 | Tera-Wasserburg concordia diagrams ($^{207}Pb/^{206}Pb$ vs. $^{238}U/^{206}Pb$) showing the results from carbonate U-Pb geochronology on samples of dolomite from the southern Rocky Mountains, western Canada (Supplementary Data 1). A, C Tera-Wasserburg diagrams for four samples of RD1 from the Cathedral Formation at the Kicking Horse Pass locality. **B, D** Tera-Wasserburg diagrams for eight samples of RD1 from the Cathedral Formation at the Whirlpool Point locality. Uncertainties were calculated as a 95% confidence interval and reported as *α* / *β*, where β includes propagated systematic uncertainties. MSWD Mean square weighted deviation. *n* = number of ablations.

geochronology (Fig. 4A–D). These Middle Cambrian to Middle Ordovician U-Pb ages indicate that dolomitization was syn- to early post-depositional, in a shallow-burial setting, which implies that there was a significant contribution from hydrothermal fluids (Fig. 5A, B).

Based on stable isotope and rare earth element analyses of Cambrian strata in western Canada, previous studies have fingerprinted the source(s) of these Mg-rich brines and demonstrated that they were a mixture between seawater and basinal fluids (e.g., crustal brines and/or evaporative brines)[23,25]. These geochemical relationships indicate that the basinal fluid interacted with ultramafic basement rocks in the deep crust, leaching minerals with particularly high Mg concentrations[23,25]. The carbonation of Mg-rich serpentine subgroup minerals ($Mg_3(Si_2O_5)(OH)_4$), for example, sequesters CO_2 by promoting the formation of dolomite and magnesite, alongside quartz and talc[23,39]. Paleoproterozoic (1.75–1.85 Ga) serpentinites have been identified in the basement rocks that underly the WCSB[40,41], which has led previous studies to invoke these crustal fluids as a source of Mg^{2+} for dolomitization[23,25].

In the case of a seawater-derived fluid, it is expected that the initial $^{207}Pb/^{206}Pb$ isotopic composition was in equilibrium with the bulk terrestrial Pb isotopic composition at the time of dolomitization. However, the initial Pb isotopic composition of RD1 (Fig. 4A–D) is more radiogenic than that predicted for bulk terrestrial Pb during the Middle Cambrian to Middle Ordovician[42]. It is possible that this is due to locally oxygenated conditions that favoured the incorporation of ^{238}U during dolomitization (which decays to ^{206}Pb, thus decreasing $^{207}Pb/^{206}Pb$)[43], but such an interpretation would discount the large volume of geochemical evidence in favour of a reduced, hydrothermal fluid that had interacted with the underlying basement rocks[23,25]. In the latter case, fluid-rock interaction could give rise to the leaching of Pb from stratigraphically older, U-bearing minerals, resulting in lower than expected $^{207}Pb/^{206}Pb$[35]. Dolomitization of Cambrian strata in western Canada is also spatially associated with Pb-Zn deposits that are located along the margin of the carbonate platform (Fig. 1B, C), but further work is required to evaluate the temporal evolution from RD1 to these later paragenetic stages[18,30]. In particular, our results from U-Pb geochronology (Fig. 4A–D) overlap with and are corroborated by Re-Os dating of the Yellowhead sulfide mineralization in northeast Washington, USA, situated in coeval strata, with a reported age of 512 ± 17 Ma[44].

Mechanisms for delivering Mg-rich brines to the seafloor

RD1 is widespread in the strata at both the Kicking Horse Pass and Mt. Stephen localities, where the sedimentary facies represent a platform margin environment and a proximal slope to basinal environment, respectively. The position and geometry of this lateral platform-to-basin transition was

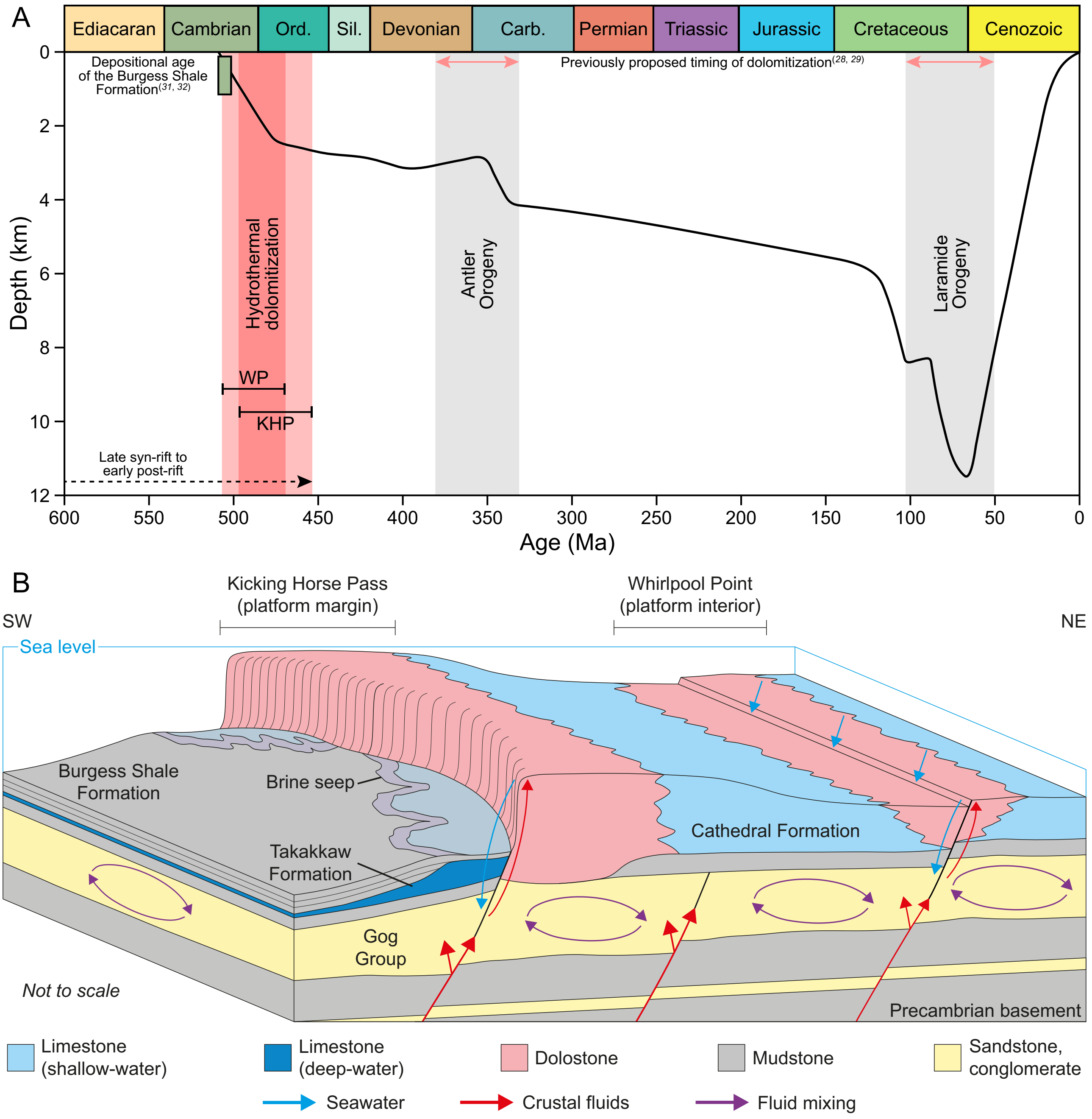

Fig. 5 | Conceptual model for the timing and mechanism of dolomitization for the Cathedral Formation and the near age-equivalent Burgess Shale Formation in western Canada. A Burial history diagram showing the timing of hydrothermal dolomitization[25,27]. Note that the depths are converted from fluid inclusion homogenization temperatures, and assume a geothermal gradient of 25 °C/km until the Laramide Orogeny and 22 °C/km thereafter[30]. Previous studies have suggested that dolomitization occurred during the Antler Orogeny[29] or the Laramide Orogeny[28], whereas our results from U-Pb geochronology demonstrate that it occurred during the Middle Cambrian to Middle Ordovician. The upper contact of Burgess Shale Formation, based on the occurrence of *Bathyuriscus*, is 507.5–501.5 Ma[32,33]. **B** Seawater and crustal fluids convected within the Gog Group (Lower Cambrian) before migrating upwards along normal-to-transtensional faults to dolomitize the Middle Cambrian strata, where these Mg-rich brines discharged along the margin of the carbonate platform.

controlled by the syndepositional reactivation of deep-rooted, basement faults in the region[15–20]. These extensional faults, oriented N-NW, also provided hydrogeological conduits for fluid flow and dolomitization. As a result, the mechanism for the dolomitization of Cambrian strata in western Canada involved the emplacement of Mg-rich, crustal fluids upwards along faults into the shallow subsurface, where they mixed with seawater and convected at temperatures up to ~200 °C (Fig. 5A, B)[23–27]. It has been demonstrated that dolomitization can occur where these hydrothermal fluids breach the seafloor along faults in extensional basins, particularly in zones of structural complexity[45,46]. Middle Cambrian to Middle Ordovician extension and the associated hydrothermal activity in western Canada was likely associated with the late syn-rift to early post-rift stages of the breakup of Rodinia and the opening of the western margin of Laurentia (Fig. 5A). In the WCSB, such rifting primarily occurred during the Neoproterozoic[47], but there is significant evidence that tectonic activity and heat flow persisted into the Cambrian[18–20,23–27]. Although these early Paleozoic structural elements have received limited attention in western Canada, there is also widespread evidence of sustained Cambrian rifting in the northern Canadian Cordillera[48,49].

Linking dolomitization with Mg-rich brine seeps in the basin

In the deep-water basin, previous studies[19–21] have proposed that Mg-rich brine seeps influenced the distribution of biota during the deposition of the Burgess Shale Formation, similar to that which occurs around modern marine mud volcanoes (Fig. 5B)[50–54]. The clinochlore geobodies on Mt. Stephen were originally thought to have resulted from the low-grade metamorphism of a seep-related protolith that comprised smectite, with lesser kaolinite and brucite[18], but recent studies have suggested that the carbonation of ultramafic basement rocks are a more likely source[21,23,25]. In modern marine settings, brine seeps are sources of reduced solutes that promote microbial productivity and concentrate animal communities in otherwise depauperate regions of the seafloor[52]. This does not necessarily require that the biota were seep obligates, which at modern seeps[54] occur at depths that are greater than that proposed for the Burgess Shale fauna[31–33]. These processes could account for the disjunct linear distribution of fossil assemblages in Middle Cambrian strata along the Cambrian platform margin, as well as the abrupt facies changes that occur along strike on Mt. Stephen (Fig. 5B)[19,20]. If this hypothesis is correct, remarkable concentrations of fauna thrived along the fault-controlled, Cathedral Escarpment, awaiting their rapid entombment to produce the preservational fidelity that is characteristic of the Burgess Shale lagerstätte[5–8].

Additional lagerstätten in Middle Cambrian strata are found in the Stanley Glacier and Marble Canyon areas of Kootenay National Park[7,8]. At Stanley Glacier, the lagerstätte is situated within the Stephen Formation in a distal ramp setting that is beyond the extent of the Cathedral Escarpment and where there is no clear influence of the exhalative, Mg-rich brines that were investigated in this study[7]. However, there are clear differences in the taxonomic composition, diversity, and density of the biota between the Stanley Glacier locality and those on Fossil Ridge that may be explained by the apparent lack of hydrothermal brine seeps. Conversely, the lagerstätte at Marble Canyon is much more analogous to those at Walcott Quarry and the Mt. Stephen Trilobite Beds, each of which are situated in the Burgess Shale Formation and are directly adjacent to the Cathedral Escarpment[8]. Nevertheless, the role of hydrothermal, Mg-rich brines in the Marble Canyon area has not yet been investigated.

Synthesis and broader implications

Using U-Pb geochronology, this interdisciplinary study shows that western Canada was tectonically active and subject to fault-controlled, hydrothermal dolomitization during the Middle Cambrian (Miaolingian Epoch) to Middle Ordovician (488.1 ± 18.8 Ma). Such hydrothermal activity indicates that the latest stages of rifting along the western margin of Laurentia persisted significantly later than previously recognized (Fig. 5A). Syn- to early post-depositional dolomitization of the Cathedral Formation also implies that cogenetic Mg-rich brines may have been mobilized from the bedrock to the seafloor during the deposition of the Burgess Shale lagerstätte (Fig. 5B). The results of this study clearly demonstrate the link between structurally controlled platform margins, fluid flux, and metasomatic reactions, while also emphasizing the importance of hydrothermal, Mg-rich brines to a major diversification event in Earth's history.

Methods

Geological setting

The WCSB is filled by a southwest-thickening wedge of sedimentary rocks, up to ~18 km thick in the southern Rocky Mountains, that extends from the southwest corner of the Northwest Territories to the northern United States (Supplementary Fig. 1A). In the southern Rocky Mountains, the WCSB includes four unconformity-bounded packages of strata that are informally divided based on their tectonic settings[55,56]. (i) The Purcell Supergroup (Mesoproterozoic) records volcanic activity and sedimentation within an intracratonic basin, whereas (ii) the Windermere Supergroup (Neoproterozoic) records the rifting of western Laurentia[55,56]. (iii) Cambrian to Triassic strata were deposited on what has historically been considered a passive margin[55–59], but there is local evidence that episodic basement reactivation gave rise to elevated heat flow throughout the Cambrian[15–21,23–27,60]. (iv) Jurassic to Paleocene strata were deposited in a foreland basin that developed during the Columbian (Jurassic to Early Cretaceous) and Laramide (Late Cretaceous to Paleocene) orogenies[61–63].

The modern structure of the southern Rocky Mountains is dominated by E–NE verging thrust faults that formed during the Antler, Columbian, and Laramide orogenies[61–63]. However, there are several pre-orogenic structural elements that have been recognized in the southern Rocky Mountains, including NE–SW trending extensional faults that intersect Middle Cambrian strata[15–20,23–27]. The most prominent of these early structural features is the Kicking Horse Rim (oriented N–NW), an elevated paleotopographic feature that formed due to the syndepositional reactivation of deep-rooted basement faults, exerting a primary control on the position of the carbonate platform margin during the Cambrian and Ordovician[15,16,57,58].

Stratigraphy

Middle Cambrian (Miaolingian Epoch) strata in the southern Rocky Mountains record a series of northeast-transgressing sedimentary cycles that comprise regionally extensive facies belts[15,16]. These cycles include a central carbonate platform-shoal complex that grades laterally into proximal slope/basinal facies to the southwest and platform/intrashelf basin facies to the northeast. Each of these carbonate platform-shoal complexes were paleogeographically confined by the tectonically active Kicking Horse Rim[15,16], and the development of each platform terminated due to the localized collapse of its basinward margin, platform drowning, and burial by siliciclastic sediment[19,33]. As a result, the sedimentary facies on Mt. Stephen (51°23′34.7“N, 116°25′39.5“W) represent proximal slope to basinal environments, whereas those at the Kicking Horse Pass locality (51°26′11.5″N, 116°22′48.5″W) represent a platform margin environment[16,33]. In contrast, the sedimentary facies at the Whirlpool Point locality (52°00′07.5″N, 116°28′13.5″W) represent a platform interior environment[15,16].

The stratigraphic nomenclature for the Cambrian strata in the southern Rocky Mountains is complicated by the different terminology on the carbonate platform relative to that in the basin (Supplementary Fig. 1B, C)[16,33]. On the platform, the Gog Group (conglomerate, sandstone, shale) is overlain by the Mt. Whyte Formation (shale, argillaceous limestone, dolomite), which interfingers with, and is overlain by the Cathedral Formation (shallow-water limestone, dolomite). The Cathedral Formation is up to ~610 m thick at its platform margin on Mt. Stephen and thins rapidly to the northeast[16]. The Cathedral Formation is overlain by the Stephen Formation (shale, argillaceous limestone), which is then overlain by the Eldon Formation (shallow-water limestone, dolomite). Towards the basin, the shallow-water platform facies of the Cathedral Formation grade laterally into the deep-water slope facies of the Takakkaw Formation (deep-water limestone, dolomite)[33,59]. These sedimentary facies changes, and the corresponding stratigraphic changes, occur at the same geographical boundary along the Kicking Horse Rim in both the underlying and overlying strata. The Stephen Formation on the platform, for example, is coeval to the Monarch Formation (mudstone, deep-water limestone, dolomite) and the Burgess Shale Formation (shale, mudstone, deep-water limestone, dolomite) in the basin (Supplementary Fig. 1B, C)[32,33]. The Monarch Formation and the Burgess Shale Formation are ~282 m thick on Mt. Stephen and Mt. Field, which were originally measured and correlated as the basinal equivalent of the Stephen Formation (Amiskwi and Wapta members)[16].

Sampling and petrographical screening

This study is based on ~270 samples, collected for 3 Ph.D. theses at The University of Manchester, that evaluated the fault-controlled, hydrothermal dolomitization of Cambrian strata in the southern Rocky Mountains[64–66]. Thus, additional field descriptions, detailed petrographical analyses, and robust geochemical data are readily available[23–27,64–66]. Prior to U-Pb geochronology, transmitted-light petrography was established on polished sections that were prepared from samples impregnated with blue-stained epoxy resin. These 30 µm thick sections were stained with alizarin red S and potassium ferricyanide[67], and then examined under plane polarized-light and between crossed-polars using a Nikon Eclipse LV100N POL microscope. These sections were then analyzed using a CITL Mk5 cold cathodoluminescence system that is mounted on the microscope (operating conditions = 15 to 20 kV, 350 to 450 µA). Dolomite crystal textures were described according to a standardized nomenclature[68].

A significant part of the petrographical screening that is described in this article concerns the effect of recrystallization (Supplementary Fig. 2A-D). It is unclear the extent to which recrystallization resets the ^{207}Pb/^{206}Pb and ^{238}U/^{206}Pb values of dolomite, but there is a large body of research demonstrating that recrystallization often overprints the petrographical and geochemical characteristics of the precursor dolomite[69–78]. In particular, recent studies have shown that dolomite recrystallization is almost ubiquitous in the geological record[77], and such processes may occur much earlier during the diagenetic history than previously recognized[78]. Recrystallization is prevalent in fault-controlled, hydrothermal dolomite bodies and is most significant proximal to the source of the dolomitizing fluid[23–27,64–66]. Results from U-Pb geochronology support such interpretations because the ages proximal to the fluid source at the Kicking Horse Pass locality are slightly younger (475.3 ± 21.8 Ma) relative to those distal to the fluid source at the Whirlpool Point locality (488.1 ± 18.8 Ma).

In situ laser ablation inductively coupled plasma mass spectrometry

Carbonate U-Pb geochronology was conducted by in-situ laser ablation inductively coupled mass spectrometry (LA ICP-MS) at the Geochronology & Tracers Facility, British Geological Survey. This method utilizes a New Wave Research 193 nm ImageGeo excimer laser ablation system fitted with a TV3 cell, which is coupled to a Nu Instruments Attom single-collector sector-field ICP-MS. The method for carbonate minerals is adapted from that which is used for zircon, with several modifications[34–38,79–84]. The laser parameters that were used are 100 µm static spots, fired at 10 Hz, with a ~ 4 J.cm^{-2} fluence, for 30 s of ablation. Transects of 26 to 28 spot ablations were carried out on each sample, parallel to depositional bedding, targeting planar-euhedral dolomite crystals that were larger than the diameter of the laser (Supplementary Fig. 2). Ablations were selected at the center of each dolomite crystal to avoid contamination from intercrystalline material (e.g., clay minerals, Pb-Zn minerals, and organic material). Sites were observed after the ablations using a binocular microscope and in reflected light (Supplementary Figs. 3, 4), and irregular ablations due to intercrystalline material, abnormalities, or crystallographic effects were culled from the dataset. Samples from the Kicking Horse Pass locality ($n = 4$) have average U and Pb concentrations (quoted alongside their standard deviation) of 175.8 ± 93.3 ppb and 384.1 ± 78.7 ppb, respectively. In contrast, samples from the Whirlpool Point locality ($n = 12$) have average U and Pb concentrations of 269.7 ± 286.1 ppb and 566.3 ± 750.9 ppb, respectively.

Standard sample bracketing uses NIST 614 glass[85] for normalization of ^{208}Pb/^{206}Pb, ^{207}Pb/^{206}Pb, and ^{238}U/^{232}Th ratios, and the internally developed WC-1 carbonate reference material[34] for ^{238}U/^{206}Pb ratios. Data reduction was conducted using the time-resolved-analysis function in the Nu Attolab software, and an internally developed excel spreadsheet. Normalization is based on the measured ratio derived from the session-based drift corrected mean of the primary WC-1 carbonate standard. No downhole correction is made because the downhole ^{238}U/^{206}Pb ratios at these ablation conditions are linear with a negligible slope. Therefore, normalization uses the mean of the ^{238}U/^{206}Pb ratios for each ablation, assuming similar ablation behavior between the samples and the reference material. No common Pb correction is made, and all the ages are determined from lower intercepts on a Tera-Wasserburg plot. In contrast to most previous publications that only use the ^{207}Pb/^{206}Pb[34] or ^{208}Pb/^{206}Pb ratios[86], we utilize the ^{208}Pb and ^{232}Th measurements[87,88] using the algorithm employed in IsoplotR[89]. This approach permits more precise measurements of the common Pb composition, which leads to more precise age estimates for data that form reasonable two-component mixtures between common Pb and radiogenic Pb. All regressions are unanchored as the spread in the data permits the accurate assessment of the common Pb component. The resulting Tera-Wasserburg concordia plots (Fig. 4A–D; Supplementary Tables 1, 2) show Model 1 ages with their respective uncertainties (95% confidence interval) quoted as α / β, where α does not include systematic uncertainties and β includes propagated systematic uncertainties. The latter incorporates the ^{238}U decay constant uncertainty, the primary reference material (WC-1) age uncertainty, and an estimate of long-term excess variance of the laboratory method[90]. A secondary carbonate reference material, Duff Brown Tank (DBT)[91], was measured to provide an additional control on accuracy and precision. The compiled data for DBT (Supplementary Fig. 5A, B) yield an age of 63.24 ± 0.91 Ma (α; without systematic uncertainties), which is within uncertainty of its isotope dilution age of 64.04 ± 0.67 Ma[91].

The method that is applied herein uses calcite ($CaCO_3$) as a reference material to analyze dolomite ($CaMg(CO_3)_2$). Consequently, a small bias in the resulting U-Pb ages may be introduced due to subtle differences between the geochemical composition and crystal structure of the samples relative to the standard, which in turn, may affect the rate of ablation and, thus, elemental fractionation. It is not precisely known how significant this bias is, but it is typically assumed to be less than a few percent, decreasing with larger spot sizes[84]. Thus, the use of a calcite reference material in dolomite U-Pb geochronology, each of which crystallizes in the trigonal crystal system, is commonplace in the geological community and the matrix effects between these minerals are generally considered to be negligible[92–96].

Data availability

The dataset supporting the findings of this study is available at: https://doi.org/10.6084/m9.figshare.25607811.v1.

Received: 13 December 2023; Accepted: 25 April 2024;

References

1. Grotzinger, J. P., Bowring, S. A., Saylor, B. Z. & Kaufman, A. J. Biostratigraphic and geochronologic constraints on early animal evolution. *Science* **270**, 598–604 (1995).
2. Maloof, A. C., Porter, S. M., Moore, J. L., Dudas, F. O., Bowring, S. A., Higgins, J. A., Fike, D. A. & Eddy, M. P. The earliest Cambrian record of animals and ocean geochemical change. *GSA Bull.* **122**, 1731–1774 (2010).
3. Fan, J. X., Shen, S. Z., Erwin, D. H., Sadler, P. M., MacLeod, N., Cheng, Q. M., Hou, X., Yang, J., Wang, X., Wang, Y., Zhang, H., Chen, X., Li, G., Zhang, Y., Shi, Y., Yuan, D., Chen, Q., Zhang, L., Li, C. & Zhao, Y. Y. A high-resolution summary of Cambrian to Early Triassic marine invertebrate biodiversity. *Science* **367**, 272–277 (2020).
4. Buatois, L. A., Mángano, M. G., Olea, R. A. & Wilson, M. A. Decoupled evolution of soft and hard substrate communities during the Cambrian Explosion and Great Ordovician Biodiversification Event. *Proc. Natl. Acad. Sci.* **113**, 6945–6948 (2016).
5. Walcott, C. D. Cambrian geology and paleontology II. Abrupt appearance of the Cambrian fauna on the North American continent. *Smithsonian Misc. Collec.* **57**, 1–16 (1910).
6. Gaines, R. R., Hammarlund, E. U., Hou, X., Qi, C., Gabbott, S. E., Zhao, Y., Peng, J. & Canfield, D. E. Mechanism for Burgess Shale-type preservation. *Proc. Natl. Acad. Sci.* **109**, 5180–5184 (2012).
7. Caron, J. B., Gaines, R. R., Mángano, M. G., Streng, M. & Daley, A. C. A new Burgess Shale–type assemblage from the “thin” Stephen Formation of the southern Canadian Rockies. *Geology* **38**, 811–814 (2010).

8. Nanglu, K., Caron, J. B. & Gaines, R. R. The Burgess Shale paleocommunity with new insights from Marble Canyon, British Columbia. *Paleobiology* **46**, 58–81 (2020).
9. Morris, S. C., Peel, J. S., Higgins, A. K., Soper, N. J. & Davis, N. C. A Burgess shale-like fauna from the Lower Cambrian of North Greenland. *Nature* **326**, 181–183 (1987).
10. Hou, X., Siveter, D. J., Siveter, D. J., Aldridge, R. J., Pei-yun, C., Gabbott, S., Xiao-ya, M., Purnell, M. A. & Williams, M. The Cambrian fossils of Chengjiang, China: the flowering of early animal life. *Oxford: Blackwell* **233**, 1–233 (2004).
11. Borgomano, J. R. F. The Upper Cretaceous carbonates of the Gargano-Murge region, southern Italy: A model of platform-to-basin transition. *AAPG Bull.* **84**, 1561–1588 (2000).
12. Eberli, G. P., Anselmetti, F. S., Betzler, C., Van Konijnenburg, J. H. & Bernoulli, D. Carbonate platform to basin transitions on seismic data and in outcrops: Great Bahama Bank and the Maiella Platform margin, Italy. In: Eberli, G. P., Masaffero, J. L. & Sarg, J. F. R. (Eds.), Seismic Imaging of Carbonate Reservoirs and Systems, *AAPG Memoir* **81**, 207–250 (2004).
13. López-Horgue, M. A., Iriarte, E., Schröder, S., Fernández-Mendiola, P. A., Caline, B., Corneyllie, H., Frémont, J., Sudrie, M. & Zerti, S. Structurally controlled hydrothermal dolomites in Albian carbonates of the Asón valley, Basque Cantabrian Basin, Northern Spain. *Marine Petroleum Geol.* **27**, 1069–1092 (2010).
14. Breislin, C., Crowley, S., Banks, V. J., Marshall, J. D., Millar, I. L., Riding, J. B. & Hollis, C. Controls on dolomitization in extensional basins: An example from the Derbyshire Platform, UK. *J. Sedimentary Res.* **90**, 1156–1174 (2020).
15. Aitken, J. D. Control of lower Paleozoic sedimentary facies by the Kicking Horse Rim, southern Rocky Mountains, Canada. *Bull. Canadian Petroleum Geol.* **19**, 557–569 (1971).
16. Aitken, J. D. Stratigraphy of the Middle Cambrian platformal succession, southern Rocky Mountains. *Geol. Survey Canada Bull.* **398**, 1–322 (1997).
17. Pratt, B. R. Teepees in peritidal carbonates: origin via earthquake-induced deformation, with example from the Middle Cambrian of western Canada. *Sedimentary Geol.* **153**, 57–64 (2002).
18. Powell, W. G., Johnston, P. A., Collom, C. J. & Johnston, K. J. Middle Cambrian brine seeps on the Kicking Horse Rim and their relationship to talc and magnesite mineralization and associated dolomitization, British Columbia, Canada. *Econ. Geol.* **101**, 431–451 (2006).
19. Johnston, P. A., Johnston, K. J., Collom, C. J., Powell, W. G. & Pollock, R. J. Palaeontology and depositional environments of ancient brine seeps in the Middle Cambrian Burgess Shale at The Monarch, British Columbia, Canada. *Palaeogeogr., Palaeoclimatol., Palaeoecol.* **277**, 86–105 (2009).
20. Johnston, P. A., Collom, C. J. & Desjardins, P. Lower to Middle Cambrian of the southern Canadian Rockies. In: Hsieh, J. C. C. (Ed.), Geologic Field Trips of the Canadian Rockies. *Geological* Society of Ame*rica Field Guide* **48**, 71-121 (2017). https://doi.org/10.1130/2017.0048(03).
21. Keith, S., Johnston, P. A., & Johnston, K. J., A serpentintite "smoking gun" in the Burgess Shale: Evidence for deep-sourced magnesium-charged hydrothermal brines and mud volcanism that fuelled the Burgess biosystem. *Geol. Soc. Am. Abs. Prog.* **49** (2017). https://doi.org/10.1130/abs/2017AM-308700.
22. Davies, G. R. & Smith, L. B. Jr Structurally controlled hydrothermal dolomite reservoir facies: An overview. *AAPG Bull.* **90**, 1641–1690 (2006).
23. Koeshidayatullah, A., Corlett, H., Stacey, J., Swart, P. K., Boyce, A., Robertson, H., Whitaker, F. & Hollis, C. Evaluating new fault-controlled hydrothermal dolomitisation models: Insights from the Cambrian Dolomite, Western Canadian Sedimentary Basin. *Sedimentology* **67**, 2945–2973 (2020).
24. Koeshidayatullah, A., Corlett, H., Stacey, J., Swart, P. K., Boyce, A. & Hollis, C. Origin and evolution of fault-controlled hydrothermal dolomitization fronts: A new insight. *Earth and Planetary Sci. Lett.* **541**, 116291 (2020).
25. Stacey, J., Corlett, H., Holland, G., Koeshidayatullah, A., Cao, C., Swart, P., Crowley, S. & Hollis, C. Regional fault-controlled shallow dolomitization of the Middle Cambrian Cathedral Formation by hydrothermal fluids fluxed through a basal clastic aquifer. *Geol. Soc. Am. Bull.* **133**, 2355–2377 (2021).
26. McCormick, C. A., Corlett, H., Stacey, J., Hollis, C., Feng, J., Rivard, B. & Omma, J. E. Shortwave infrared hyperspectral imaging as a novel method to elucidate multi-phase dolomitization, recrystallization, and cementation in carbonate sedimentary rocks. *Sci. Rep.* **11**, 1–16 (2021).
27. McCormick, C. A., Corlett, H., Clog, M., Boyce, A. J., Tartese, R., Steele-MacInnis, M. & Hollis, C. Basin scale evolution of zebra textures in fault-controlled, hydrothermal dolomite bodies: Insights from the Western Canadian Sedimentary Basin. *Basin Res.* **35**, 2010–2039 (2023).
28. Symons, D. T. A., Lewchuk, M. T. & Sangster, D. F. Laramide orogenic fluid flow into the Western Canada sedimentary basin; evidence from paleomagnetic dating of the Kicking Horse mississippi valley-type ore deposit. *Econ. Geol.* **93**, 68–83 (1998).
29. Vandeginste, V., Swennen, R., Gleeson, S. A., Ellam, R. M., Osadetz, K. & Roure, F. Zebra dolomitization as a result of focused fluid flow in the Rocky Mountains Fold and Thrust Belt, Canada. *Sedimentology* **52**, 1067–1095 (2005).
30. Vandeginste, V., Swennen, R., Gleeson, S. A., Ellam, R. M., Osadetz, K. & Roure, F. Geochemical constraints on the origin of the Kicking Horse and Monarch Mississippi Valley-type lead-zinc ore deposits, southeast British Columbia, Canada. *Mineralium Deposita* **42**, 913–935 (2007).
31. Stewart, W. D., Dixon, O. A. & Rustt, B. R. Middle cambrian carbonate-platform collapse, southeastern Canadian rocky mountains. *Geology* **21**, 687–690 (1993).
32. Fletcher, T. P. & Collins, D. H. The middle Cambrian Burgess Shale and its relationship to the Stephen Formation in the southern Canadian Rocky Mountains. *Canadian J. Earth Sci.* **35**, 413–436 (1998).
33. Collom, C. J., Johnston, P. A. & Powell, W. G. Reinterpretation of 'Middle' Cambrian stratigraphy of the rifted western Laurentian margin: Burgess Shale Formation and contiguous units (Sauk II megasequence), Rocky Mountains, Canada. *Palaeogeogr., Palaeoclimatol., Palaeoecol.* **277**, 63–85 (2009).
34. Roberts, N. M., Rasbury, E. T., Parrish, R. R., Smith, C. J., Horstwood, M. S. & Condon, D. J. A calcite reference material for LA-ICP-MS U-Pb geochronology. *Geochem., Geophys., Geosyst.* **18**, 2807–2814 (2017).
35. Roberts, N. M., Drost, K., Horstwood, M. S., Condon, D. J., Chew, D., Drake, H., Milodowski, A. E., McLean, N. M., Smye, A. J., Walker, R. J., Haslam, R., Hodson, K., Imber, J., Beaudoin, N. & Lee, J. K. Laser ablation inductively coupled plasma mass spectrometry (LA-ICP-MS) U–Pb carbonate geochronology: strategies, progress, and limitations. *Geochronology* **2**, 33–61 (2020).
36. Elisha, B., Nuriel, P., Kylander-Clark, A. & Weinberger, R. Towards in situ U–Pb dating of dolomite. *Geochronology* **3**, 337–349 (2021).
37. Gasparrini, M., Morad, D., Mangenot, X., Bonifacie, M., Morad, S., Nader, F. H. & Gerdes, A. Dolomite recrystallization revealed by Δ_{47}/U-Pb thermochronometry in the Upper Jurassic Arab Formation, United Arab Emirates. *Geology* **51**, 471–475 (2023).
38. Xiao, D., Huang, T., Xu, Q., Tan, X., Wen, L., Zheng, J. & Cao, J. Two pulsed activities of the Emeishan large igneous province in southwestern China inferred from dolomite U-Pb geochronology and significance. *Geol. Soc. Am. Bull.* https://doi.org/10.1130/B37302.1 (2024).

39. Hansen, L. D., Dipple, G. M., Gordon, T. M. & Kellett, D. A. Carbonated serpentinite (listwanite) at Atlin, British Columbia: A geological analogue to carbon dioxide sequestration. *Canadian Mineralogist* **43**, 225–239 (2005).
40. Eaton, D. W. & Cassidy, J. F. A relic Proterozoic subduction zone in western Canada: New evidence from seismic reflection and receiver function data. *Geophys. Res. Letters* **23**, 3791–3794 (1996).
41. Gu, Y. J., Chen, Y., Dokht, R. M. & Wang, R. Precambrian tectonic discontinuities in western Laurentia: Broadband seismological perspectives on the Snowbird and Great Falls tectonic zones. *Tectonics* **37**, 1411–1434 (2018).
42. Stacey, J. S. & Kramers, J. D. Approximation of terrestrial lead isotope evolution by a two-stage model. *Earth and Planetary Science Letters* **26**, 207–221 (1975).
43. Ben-Israel, M., Holder, R. M., Nelson, L. L., Smith, E. F., Kylander-Clark, A. R. & Ryb, U. Late Paleozoic oxygenation of marine environments supported by dolomite U-Pb dating. *Nat. Commun.* **15**, 2892 (2024).
44. Paradis, S., Hnatyshin, D., Simandl, G. J. & Creaser, R. A. Re-Os pyrite geochronology of the yellowhead-type mineralization, pend oreille mine, Kootenay Arc, Metaline District, Washington. *Econ. Geol.* **115**, 1373–1384 (2020).
45. Hollis, C., Bastesen, E., Boyce, A., Corlett, H., Gawthorpe, R., Hirani, J., Rotevatn, A. & Whitaker, F. Fault-controlled dolomitization in a rift basin. *Geology* **45**, 219–222 (2017).
46. Benjakul, R., Hollis, C., Robertson, H. A., Sonnenthal, E. L. & Whitaker, F. F. Understanding controls on hydrothermal dolomitisation: insights from 3D reactive transport modelling of geothermal convection. *Solid Earth* **11**, 2439–2461 (2020).
47. Colpron, M., Logan, J. M. & Mortensen, J. K. U–Pb zircon age constraint for late Neoproterozoic rifting and initiation of the lower Paleozoic passive margin of western Laurentia. *Canadian J. Earth Sci.* **39**, 133–143 (2002).
48. Moynihan, D. P., Strauss, J. V., Nelson, L. L. & Padget, C. D. Upper Windermere Supergroup and the transition from rifting to continent-margin sedimentation, Nadaleen River area, northern Canadian Cordillera. *GSA Bull.* **131**, 1673–1701 (2019).
49. Busch, J. F., Rooney, A. D., Meyer, E. E., Town, C. F., Moynihan, D. P. & Strauss, J. V. Late Neoproterozoic–early Paleozoic basin evolution in the Coal Creek inlier of Yukon, Canada: implications for the tectonic evolution of northwestern Laurentia. *Canadian J. Earth Sci* **58**, 355–377 (2021).
50. Paull, C. K., Hecker, B., Commeau, R., Freeman-Lynde, R. P., Neumann, C., Corso, W. P., Golubic, S., Hook, J. E., Sikes, E. & Curray, J. Biological communities at the Florida Escarpment resemble hydrothermal vent taxa. *Science* **226**, 965–967 (1984).
51. Tyler, P. A. & Young, C. M. Dispersal at hydrothermal vents: a summary of recent progress. *Hydrobiologia* **503**, 9–19 (2003).
52. Olu-Le Roy, K., Sibuet, M., Fiala-Médioni, A., Gofas, S., Salas, C., Mariotti, A., Foucher, J. & Woodside, J. Cold seep communities in the deep eastern Mediterranean Sea: composition, symbiosis and spatial distribution on mud volcanoes. *Deep Sea Res. Part I: Oceanogr. Res. Papers* **51**, 1915–1936 (2004).
53. Joye, S. B., Samarkin, V. A., Orcutt, B. N., MacDonald, I. R., Hinrichs, K. U., Elvert, M., Teske, A. P., Lloyd, K. G., Lever, M. A., Montoya, J. P. & Meile, C. D. Metabolic variability in seafloor brines revealed by carbon and sulphur dynamics. *Nat. Geosci.* **2**, 349–354 (2009).
54. Dando, P. R. Biological communities at marine shallow-water vent and seep sites. In: Kiel, S. (Ed.), The Vent and Seep Biota–From Microbes to Ecosystems. *Topics in Geomicrobiology* **33**, 333-378 (2010).
55. Bond, G. C. & Kominz, M. A. Construction of tectonic subsidence curves for the early Paleozoic miogeocline, southern Canadian Rocky Mountains: Implications for subsidence mechanisms, age of breakup, and crustal thinning. *Geol. Soc Am. Bull.* **95**, 155–173 (1984).
56. Desjardins, P. R., Buatois, L. A., Pratt, B. R. & Mángano, M. G. Stratigraphy and sedimentary environments of the Lower Cambrian Gog Group in the southern Rocky Mountains of Western Canada: Transgressive sandstones on a broad continental margin. *Bull. Canad. Petroleum Geol.* **58**, 403–439 (2010).
57. Aitken, J. D. Birth, growth and death of the Middle Cambrian Cathedral carbonate lithosome, Southern Rocky Mountains. *Bull. Canad. Petroleum Geol.* **37**, 316–333 (1989).
58. Slind, O. L., Andrews, G. D., Murray, D. L., Norford, B. S., Paterson, D. F., Salas, C. J. & Tawadros, E. E. Middle Cambrian to lower Ordovician strata of the Western Canada Sedimentary Basin. In: Mossop, G. & Shetsen, I. (Eds.), Geological atlas of the Western Canada Sedimentary Basin. *Canadian Society of Petroleum Geologists and Alberta Research Council Special Report* **4**, 87–108 (1994).
59. Fletcher, T. P. & Collins, D. H. The Burgess Shale and associated Cambrian formations west of the Fossil Gully Fault Zone on Mount Stephen, British Columbia. *Canadian J. Earth Sci.* **40**, 1823–1838 (2003).
60. Bond, G. C., Christie-Blick, N., Kominz, M. A. & Devlin, W. J. An early Cambrian rift to post-rift transition in the Cordillera of western North America. *Nature* **315**, 742–746 (1985).
61. Price, R. The cordilleran foreland thrust and fold belt in the southern Canadian Rocky Mountains. *Geol. Soc. London Special Publ.* **9**, 427–448 (1981).
62. Root, K. G. Devonian Antler fold and thrust belt and foreland basin development in the southern Canadian Cordillera: Implications for the Western Canada Sedimentary Basin. *Bull. Canad. Petroleum Geol.* **49**, 7–36 (2001).
63. McMechan, M. E. Structural geometry and kinematic history of the southern Kicking Horse Rim Cambrian carbonate platform: Out-of-sequence thrust faulting in the southern Canadian Rocky Mountains. *Bulletin of Canadian Petroleum Geology* **69**, 51–72 (2022).
64. Koeshidayatullah, A. Determination of the processes governing the termination of fault-controlled dolostone bodies. *Doctoral Dissertation, The University of Manchester*, 1–287 (2019).
65. Stacey J., Determination of basin-scale fluid flux to understand the processes controlling regional dolomitization in the western Canada sedimentary basin. *Doctoral Dissertation, The University of Manchester*, 1–347 (2021).
66. McCormick, C. A. Diagnostic rock textures in fault-controlled dolomite bodies: insights from hyperspectral imaging and the integration of petrographical, geochemical, and geomechanical analyses. *Doctoral Dissertation, The University of Manchester*, 1–276 (2023).
67. Dickson, J. A. D. Carbonate identification and genesis as revealed by staining. *J. Sediment. Res.* **36**, 491–505 (1966).
68. Sibley, D. F. & Gregg, J. M. Classification of dolomite rock textures. *J. Sediment. Res.* **57**, 967–975 (1987).
69. Gregg, J. M., Howard, S. A. & Mazzullo, S. J. Early diagenetic recrystallization of Holocene (< 3000 years old) peritidal dolomites, Ambergris Cay, Belize. *Sedimentology* **39**, 143–160 (1992).
70. Malone, M. J., Baker, P. A. & Burns, S. J. Recrystallization of dolomite: evidence from the Monterey Formation (Miocene), California. *Sedimentology* **41**, 1223–1239 (1994).
71. Machel, H. G. Recrystallization versus neomorphism, and the concept of ‘significant recrystallization’ in dolomite research. *Sedimentary Geol.* **113**, 161–168 (1997).
72. Al-Aasm, I. S. & Packard, J. J. Stabilization of early-formed dolomite: a tale of divergence from two Mississippian dolomites. *Sedimentary Geol.* **131**, 97–108 (2000).
73. Fu, Q., Qing, H. & Bergman, K. M. Early dolomitization and recrystallization of carbonate in an evaporite basin: the Middle

Devonian Ratner laminite in southern Saskatchewan, Canada. *J. Geol. Soc.* **163**, 937–948 (2006).
74. Rott, C. M. & Qing, H. Early dolomitization and recrystallization in shallow marine carbonates, Mississippian Alida Beds, Williston Basin (Canada): evidence from petrography and isotope geochemistry. *J. Sediment. Res.* **83**, 928–941 (2013).
75. Malone, M. J., Baker, P. A. & Burns, S. J. Recrystallization of dolomite: An experimental study from 50-200 °C. *Geochimica et Cosmochimica Acta* **60**, 2189–2207 (1996).
76. Kaczmarek, S. E. & Sibley, D. F. Direct physical evidence of dolomite recrystallization. *Sedimentology* **61**, 1862–1882 (2014).
77. Manche, C. J. & Kaczmarek, S. E. A global study of dolomite stoichiometry and cation ordering through the Phanerozoic. *J. Sediment. Res.* **91**, 520–546 (2021).
78. Ryan, B. H., Kaczmarek, S. E., Rivers, J. M. & Manche, C. J. Extensive recrystallization of Cenozoic dolomite during shallow burial: A case study from the Palaeocene–Eocene Umm er Radhuma formation and a global meta-analysis. *Sedimentology* **69**, 2053–2079 (2022).
79. Li, Q., Parrish, R. R., Horstwood, M. S. A. & McArthur, J. M. U–Pb dating of cements in Mesozoic ammonites. *Chem. Geol.* **376**, 76–83 (2014).
80. Spencer, C. J., Roberts, N. M. W., Cawood, P. A., Hawkesworth, C. J., Prave, A. R., Antonini, A. S. M. & Horstwood, M. S. A. Intermontane basins and bimodal volcanism at the onset of the Sveconorwegian Orogeny, southern Norway. *Precambrian Res.* **252**, 107–118 (2014).
81. Coogan, L. A., Parrish, R. R. & Roberts, N. M. Early hydrothermal carbon uptake by the upper oceanic crust: Insight from in situ U-Pb dating. *Geology* **44**, 147–150 (2016).
82. Roberts, N. M. & Walker, R. J. U-Pb geochronology of calcite-mineralized faults: Absolute timing of rift-related fault events on the northeast Atlantic margin. *Geology* **44**, 531–534 (2016).
83. Beaudoin, N., Lacombe, O., Roberts, N. M. & Koehn, D. U-Pb dating of calcite veins reveals complex stress evolution and thrust sequence in the Bighorn Basin, Wyoming, USA. *Geology* **46**, 1015–1018 (2018).
84. Rochelle-Bates, N., Roberts, N. M. W., Sharp, I., Freitag, U., Verwer, K., Halton, A., Fiordalisi, E., van Dongen, B. E., Swart, R., Ferreira, C. H., Dixon, R. & Schröder, S. Geochronology of volcanically associated hydrocarbon charge in the pre-salt carbonates of the Namibe Basin, Angola. *Geology* **49**, 335–340 (2021).
85. Woodhead, J. D. & Hergt, J. M. Strontium, neodymium and lead isotope analyses of NIST glass certified reference materials: SRM 610, 612, 614. *Geostandards Newslett.* **25**, 261–266 (2001).
86. Parrish, R. R., Parrish, C. M. & Lasalle, S. Vein calcite dating reveals Pyrenean orogen as cause of Paleogene deformation in southern England. *J. Geol. Soc.* **175**, 425–442 (2018).
87. Vermeesch, P. Unifying the U–Pb and Th–Pb methods: joint isochron regression and common Pb correction. *Geochronology* **2**, 119–131 (2020).
88. Liivamägi, S., Środoń, J., Bojanowski, M. J., Stanek, J. J. & Roberts, N. M. W. Precambrian paleosols on the Great Unconformity of the East European Craton: an 800 million year record of Baltica's climatic conditions. *Precambrian Res.* **363**, 106327 (2021).
89. Vermeesch, P. IsoplotR: A free and open toolbox for geochronology. *Geosci. Front.* **9**, 1479–1493 (2018).
90. Horstwood, M. S., Košler, J., Gehrels, G., Jackson, S. E., McLean, N. M., Paton, C., Pearson, N. J., Sircombe, K., Sylvester, P., Vermeesch, P., Bowring, J. F., Condon, D. J. & Schoene, B. Community-derived standards for LA-ICP-MS U-(Th-) Pb geochronology–Uncertainty propagation, age interpretation and data reporting. *Geostandards and Geoanalytical Research* **40**, 311–332 (2016).
91. Hill, C. A., Polyak, V. J., Asmerom, Y. & Provencio, P. P. Constraints on a Late Cretaceous uplift, denudation, and incision of the Grand Canyon region, southwestern Colorado Plateau, USA, from U-Pb dating of lacustrine limestone. *Tectonics* **35**, 896–906 (2016).
92. Jiang, L., Shen, A., Wang, Z., Hu, A., Wang, Y., Luo, X., Liang, F., Azmy, K. & Pan, L. U–Pb geochronology and clumped isotope thermometry study of Neoproterozoic dolomites from China. *Sedimentology* **69**, 2925–2945 (2022).
93. Su, A., Chen, H., Feng, Y. X., Zhao, J. X., Wang, Z., Hu, M., Jiang, H. & Nguyen, A. D. In situ U-Pb dating and geochemical characterization of multi-stage dolomite cementation in the Ediacaran Dengying Formation, Central Sichuan Basin, China: Constraints on diagenetic, hydrothermal and paleo-oil filling events. *Precambrian Res.* **368**, 106481 (2022).
94. Xiong, S. F., Jiang, S. Y., Zhao, J. X., Niu, P. P., Ma, Y. & Bai, X. Y. Dating Precambrian sedimentary carbonate strata by in situ U–Pb isotopes of dolomite. *Precambrian Res.* **393**, 107088 (2023).
95. Hodgskiss, M. S., Roberts, N. M., Päiste, P., Rameil, N., Hammer, E., Brunstad, H. & Lepland, A. Direct dating of deposition and rift-related alteration of fossil barren red bed units in the North Sea. *J. Geol. Soc.***181**, jgs2023–jgs2052 (2023).
96. Rochelle-Bates, N., Wood, R., Schröder, S. & Roberts, N. M. In situ U–Pb geochronology of Pre-Salt carbonates reveals links between diagenesis and regional tectonics. *Terra Nova* **34**, 271–277 (2022).

Acknowledgements

We are grateful to The University of Manchester for President's Doctoral Scholar awards to C.A.M. and A.K., as well as to the Natural Environment Research Council (NERC) Centre for Doctoral Training for grant NE/M00578X/1 to J.S. U-Pb geochronology was funded by a NERC National Environmental Isotope Facility grant 2523.0422 to C.A.M. and C.H. Additional support came from The Geological Society of London research grant to C.A.M. and the Natural Sciences and Engineering Research Council of Canada grant 244503 to P.A.J. and C.J.C. Research and collection permits were provided by Parks Canada and Alberta Tourism, Parks and Recreation. Lastly, we greatly appreciate the careful reviews that were provided by two anonymous reviewers on an earlier version of this manuscript.

Author contributions

Conceptualization: C.A.M.; Methodology: C.A.M., N.M.W.R.; Investigation: C.A.M.; Visualization: C.A.M., P.J., C.J.C., J.S.; Funding acquisition: C.A.M., C.H.; Project administration: H.J.C., C.H.; Supervision: H.J.C., C.H.; Writing – original draft: C.A.M.; Writing – review & editing: H.J.C., N.M.W.R., P.J., C.J.C., J.S., A.K., C.H.

Competing interests

The authors declare no competing interests.

Additional information

Supplementary information The online version contains supplementary material available at https://doi.org/10.1038/s43247-024-01429-0.

Correspondence and requests for materials should be addressed to Cole A. McCormick.

Peer review information *Communications Earth & Environment* thanks the anonymous reviewers for their contribution to the peer review of this work. Primary Handling Editors: João Duarte and Carolina Ortiz Guerrero. A peer review file is available.